Quality Assessment of Despeckled SAR Images

Silvana G. Dellepiane, *Member, IEEE*, and Elena Angiati

Abstract—In this paper, a novel method for the quality assessment of despeckled SAR images is proposed. This method is based on the observation that the perceived quality of despeckled SAR images is not always appropriately described by classical statistical and deterministic parameters that are proposed in the literature. Various evaluations are performed here. A preliminary visual qualitative evaluation is taken as a reference for the subsequent quantitative assessment. Then, a revised statistical analysis that can solve some of the drawbacks of previous methods is proposed; however, the statistical approach still has certain drawbacks. To address this problem, a new frequency analysis approach is first proposed, together with a definition of the appropriate indexes. In this way, it is possible to select the best filter in terms of noise reduction, edge and texture preservation, while limiting the effect of introduced distortions. While statistical analysis is widely used in the literature, frequency analysis has never been presented for this aim, especially for non-linear filters. We prove that frequency analysis can robustly identify the best filter, taking perceptual considerations into account, even when statistical analysis fails. Despeckling methods based on anisotropic diffusion algorithms are used for a comparison, but the proposed analysis can be applied to any filtering method. Experiments are presented with SAR images from the Italian Cosmo/Skymed constellation. Both Stripmap and Spotlight acquisitions have been evaluated, and to prove the validity of the proposed method with respect to different spatial resolutions and different classes of interest, various classes are considered.

Index Terms—Adaptive filters, anisotropic diffusion, despeckling, frequency analysis, SAR images, statistical analysis.

I. INTRODUCTION

S PECKLE is responsible for the granularity of coherent imaging systems such as radar, laser, ultrasound, and Synthetic Aperture Radar (SAR). It is a scattering phenomenon that results from limited sensor resolution with respect to the individual scatter that contributes to an image pixel, and it is caused by coherent processing of backscattered signals from multiple distributed targets.

Speckle is often considered to be "multiplicative noise", but it is not just noise, as it brings significant information about the scene under investigation. Examples in which speckle preservation is important include feature-tracking in ultrasound imaging and the detection of features that are of the same scale as the speckle patterns (e.g., coagulation damage in hematology). In general, speckle reduction is mainly desired as a preparation phase before image analysis steps such as feature detection [1], segmentation [2], and classification [3].

Despite the fact that speckle is related to all of the aforementioned coherent imaging systems mentioned before, speckle-reducing filters have mainly originated in the SAR community.

Non-linear filters are the major denoising filters applied in the processing of real digital images. In this work, various adaptive algorithms for despeckling already presented in the literature are compared with the most recent method, which is based on anisotropic diffusion. The originally proposed quality assessment approach is aimed at becoming a general procedure that can be applied to images that are filtered with any other despeckling algorithms.

The aim of this paper is to overcome the classical drawbacks of the existing quality assessment approaches for despeckled SAR images. New quantitative assessment measures based on statistical analysis are originally proposed as an extension of existing statistical parameters and to select the filter that presents the best performance in terms of both noise reduction and detail preservation at the same time.

Initially, we have performed a qualitative evaluation through visual interpretation, followed by the investigation of quantitative assessments through both statistical and frequency analysis. We have proven that statistical analysis does not always allow us to identify the best filter, although this approach is extensively used in literature. We have instead considered analysis in the frequency domain, which is very innovative because it has never been proposed in the literature, and it is proven capable of establishing the effectiveness of the best filter. Quantitative measurements within the frequency domain have been performed and are presented here to demonstrate the effectiveness of this approach. To this end, we have introduced some new numerical parameters and analysis functions to validate the performance of filtering methods and to allow for an objective comparison.

Section II is a general overview of the proposed approach and introduces the methods applied, the datasets, and the objectives. Section III describes the statistical basis for the SAR image models, as related to the local characteristics that are to be optimized by the adaptive filter procedures. The most commonly applied despeckling methods are briefly introduced.

Section IV reviews the statistical parameters that are currently in use for the evaluation of despeckling method performances. Section V describes, in detail, the proposed evaluation parameters, starting with some revised statistical parameters, and followed by a new frequency analysis approach.

The experimental results are presented in Section VI, where the quality evaluation metrics proposed applied to real SAR images and a discussion of the results and the validity of the approach are presented. Conclusions and final remarks are presented in Section VII.

II. OVERVIEW OF THE PROPOSED METHOD

In the literature, few methods are described that quantitatively assess filtered images according to various aspects such as noise reduction, edges and feature preservation. Because they address statistical and deterministic evaluation metrics, the results of these methods can be contradictory and often do not appropriately reproduce human perceptual interpretation.

In general, the performances of de-speckling filters are quantitatively evaluated only on simulated images. From experimental results, it is not always possible to identify the best filter. More often, the evaluation of the results obtained from real images is only visually achieved.

An innovative approach is proposed here as an extension of traditional evaluation methods, analyzing the effects of the algorithms on the processed image. To overcome the problems of the deterministic and statistical approaches, we propose a frequency analysis based on a comparison between the spectra of the original image and the filtered image. New indexes that can gain quantitative evidence of the visual comparison are then proposed.

The best known de-speckling filters that exist in the literature and in commercial tools will be compared with the quite recent Speckle-Reducing-Anisotropic-Diffusion (SRAD) approach [4]. This filter not only preserves but also enhances edges by inhibiting diffusion across the edges and allowing diffusion on either side of the edge. Moreover, it is adaptive and does not utilize hard thresholds to alter performance in homogeneous regions or near edges and small features.

As described by Yu and Acton [4], the classical Lee and Frost filters, Enhanced Lee and Enhanced Frost filters can be expressed by partial-differential equations and can be posed as discrete isotropic diffusion methods. The following analysis is focused on this class of filters. For a comparison of classical filters with other approaches, such as wavelet-based methods [18], the reader is referred to a previous paper [5].

The quality assessment approach proposed and described herein should be applied to obtain quantitative evidence of the visual comparison of generic image processing methods without the need for simulated data or ground-truth images.

III. IMAGE DESPECKLING

Radar waves can interfere constructively or destructively to produce the well-known speckle phenomenon. In SAR imaging, this issue is a major source of problems for image analysis and interpretation processes. Reducing the effect of the speckling allows for both better discrimination of the scene targets and easier automatic image processing.

A SAR resolution cell is very large when compared to the wavelength of the illuminating electromagnetic wave. The image generation involves coherent processing that is performed on the received signal.

The SAR image value at each pixel is a function of the Radar Cross Section (RCS), σ, which is a measure of the local reflectivity of the target; this reflectivity depends on the target's backscattering properties. Given the complex backscattering signal at pixel coordinate (x, y), the two basic SAR imaging products are the Amplitude $A(x, y)$ (Single Look) and the Phase, $\varphi(x, y)$. The (Single-Look) Intensity Image, named the "power image", is defined as follows:

$$I(x, y) = A^2(x, y). \tag{1}$$

At each pixel, the value of the power image is usually considered to be the best RCS, σ, estimate. As is well known for single-look images, a model of the power image in a homogeneous area has a negative exponential distribution, the statistical parameters of which depend on the target area's physical and electromagnetic characteristics in addition to the incident wave features.

For the goal of signal processing, the product model describes the signal power as a backscattering coefficient value, σ, that is multiplied by an independent random speckle, $n_I(x, y)$:

$$I(x, y) = \sigma(x, y) \cdot n_I(x, y). \tag{2}$$

Depending on the imaged terrain class, the backscattering coefficient value, σ, is deterministic. The speckle is usually considered to be a stationary random process in homogeneous areas and follows an exponential model with a unitary mean and unitary variance in single-look Intensity images, $n_I(x, y)$.

From among the features that were proposed to evaluate the SAR image quality, the inherent signal-to-noise ratio (ISNR) for power detection was defined by [6] as the following:

$$ISNR_I = \frac{mean^2(I(x, y))}{\text{var}(I(x, y))}. \tag{3}$$

It is easy to derive that $ISRN_{nI}$ (defined as $ISNR_{nI} = mean^2(n_I(x, y))/\text{var}(n_I(x, y))$) and $ISNR_I$ are both independent from the RCS value and both have unit values.

The observed single-look amplitude at each pixel, given σ, has the conditional probability density function (pdf):

$$p_A(A \,|\, \sigma) = \frac{2A}{\sigma^2} \exp\left(-\frac{A^2}{\sigma^2}\right) \cdot u(A) \tag{4}$$

where $u(A)$ is the step function.

Following again the product model, one can find that the speckle in amplitude SAR images $(n_A(x, y))$, which is defined by the following:

$$A(x, y) = \sqrt{\sigma(x, y) \cdot n_I(x, y)} = \sqrt{\sigma(x, y)} \cdot n_A(x, y) \tag{5}$$

is Rayleigh distributed, with a mean value and variance equal to the following:

$$\overline{A} = \frac{\sqrt{\pi}\sigma}{2}, \qquad \mu_2 = \frac{4 - \pi}{4}\sigma. \tag{6}$$

As a consequence, the $ISNR_{nA}$ and $ISNR_A$ are again independent from the RCS value, and they always assume the following value:

$$ISNR_{nA} = ISNR_A = \frac{\pi}{4 - \pi} \cong 3.659. \tag{7}$$

The primary SAR de-speckling approach is "multi-looking processing", based on incoherent averaging of different images ("image looks" or "looks") that are generated by separately processed non-overlapping parts of the SAR data spectrum [7].

For L-look images, the intensity value $I(x, y)$ can be represented as the product of the Radar Cross Section with a speckle contribution $n_{IL}(x, y)$, which becomes a unit mean gamma distributed process with an order parameter L. Its pdf is then given by the following:

$$p_{nIL}(n) = \frac{L^L n^{L-1}}{\Gamma(L)} \exp(-Ln), \quad n \geq 0. \quad (8)$$

In this case, the mean value, μ_{nIL}, is equal to I and the variance, σ^2_{nIL}, is equal to $1/L$. Because $ISNR_{nIL} = L$, the quality increased $10 Log(L)$ decibels compared to the single-look intensity data.

However, multi-looking is equivalent to the linear moving-average filter; therefore, it blurs edges, decreases the image resolution, and causes an irreversible loss in the image features. Consequently, new methods are continuously under study with the aim of removing the speckle without blurring and without destroying important image features. For this purpose, the non-linear, adaptive filtering approach has appeared in the literature starting in the 1980s.

The most widely cited and applied adaptive de-speckling filters in the SAR community include the Lee [8], [9], Frost [10], Kuan and Gamma MAP filters [11]. More recently, based on the PDE approach, the new method of Speckle-Reducing-Anisotropic-Diffusion (SRAD) has been proposed and is applied here and evaluated comparatively on real images [4].

In the medical application domain, the most recent proposals for filtering ultrasound images are based on complex wavelets [12] and on wavelet diffusion [13].

In general, the performances of such filters are quantitatively evaluated only on simulated images by analyzing deterministic and statistical filter properties. The evaluation of results obtained from real images is seldom presented and is very often only visually achieved. An exception is described in [20], which addresses Magnetic Resonance Imaging, in which the noise-free image is obtained by averaging four repeated measurements.

The consolidated Lee, Frost, and Kuan algorithms balance the local application of averaging and all-pass filtering, depending on the inside characteristics of the moving window. To this end, the coefficient of variation is defined. Given a region r, of size $D(r)$, in the generic image $M(x, y)$, we make use of the region sample mean μ_{Mr}, and the corrected sample variance s^2_{Mr}, which are defined as follows:

$$\mu_{Mr} = \frac{1}{D(r)} \sum_{i \in r} M(x_i, y_i),$$

$$s_{Mr}^2 = \frac{1}{D(r) - 1} \sum_{i \in r} [M(x_i, y_i) - \mu_{Mr}]^2. \quad (9)$$

In [14], the region Coefficient of Variation (CV) is derived as the following:

$$CV_{Mr} = \frac{\sqrt{s_{Mr}^2}}{\mu_{Mr}} = \frac{s_{Mr}}{\mu_{Mr}}. \quad (10)$$

In a similar way, in a generic image $M(x, y)$, given a neighborhood of pixel (x_a, y_a), namely $\xi(x_a, y_a)$, of size $D(\xi)$, after defining the a-neighborhood sample mean μ_{Ma} and the neighborhood corrected sample variance s^2_{Ma}, the local Coefficient of Variation is:

$$\mu_{Ma} = \frac{1}{D(\xi)} \sum_{i \in \xi(x_a, y_a)} M(x_i, y_i),$$

$$s_{Ma}^2 = \frac{1}{D(\xi) - 1} \sum_{i \in \xi(x_a, y_a)} [M(x_i, y_i) - \mu_{Ma}]^2 \quad (11)$$

$$CV_{Ma} = \frac{s_{Ma}}{\mu_{Ma}}. \quad (12)$$

The Lee and Kuan filters have the same formation, although the signal model assumptions and the derivations are different. Essentially, they form an output image by computing a linear combination of the center pixel intensity with the average intensity of the window. The linear combination depends on a comparison of the local coefficient of variation, computed as in (12), with the speckle CV. The filters achieve a balance between straightforward averaging (in homogeneous regions) and the identity filter (where edges and point features are present).

The Frost filter strikes a balance between averaging and the all-pass filter. In this case, the balance is achieved by forming an exponentially-shaped filter kernel that can vary from a basic average filter to an identity filter on a point-wise, adaptive, basis. Again, the response of the filter varies locally with the coefficient of variation. In cases with a low coefficient of variation, the filter is more of an average type; in cases with a high coefficient of variation, the filter attempts to preserve sharp features by avoiding averaging. As described by Yu and Acton [4], although these despeckling filters are named "edge-preserving" and "feature-preserving," they have major drawbacks. They are sensitive to the size and shape of the filter window. Given a too-large filter window, over-smoothing occurs and edges are blurred. In contrast, a small window will leave a speckle unchanged. Because they apply a square window, corners of rectangular features are rounded and blocking artifacts occur.

It has been already proven [4], that these filters do not enhance edges; they only inhibit smoothing near edges because the coefficient of variation is high in their neighborhood. In addition, they are not directional. In the vicinity of an edge, all smoothing is precluded, instead of inhibiting smoothing in directions perpendicular to the edge and encouraging smoothing in directions parallel to the edge.

The extended versions of the Lee filter and the Frost filter [11] have been introduced to locally improve performances according to three cases. In the first case, pure averaging is induced when the local coefficient of variation is below a lower threshold. Above a higher threshold, the filter performs as a strict all-pass (identity) filter. When the coefficient of variation exists between the two thresholds, a balance between averaging and the identity is computed (as with the standard Lee and Frost filters). Such a design of enhanced filters does not definitively solve the drawbacks of the original approaches, and a robust solution is not found. In all cases, we must finally notice that serious blotching artifacts arise.

Both the Lee and Frost filters can be expressed by partial-differential equations and can be posed as discrete isotropic diffusion methods. The PDE-based filter approach allows the generation of an image scale-space without a bias from the filter window size and shape. From these considerations, the Speckle Reducing Anisotropic Diffusion (SRAD) framework has been derived [4].

SRAD not only preserves edges but also enhances edges by inhibiting diffusion across edges and allowing diffusion on either side of the edge. SRAD is adaptive and does not utilize hard thresholds to alter the performance in homogeneous regions or in regions near edges and small features.

The new diffusion technique is based on the same minimum mean square error (MMSE) approach to filtering as the Lee (Kuan) and Frost filters. Therefore, SRAD is considered to be the edge-sensitive extension of conventional adaptive speckle filters, in the same way that original Perona and Malik anisotropic diffusion [15] is the edge-sensitive extension of the average filter. In this new method, adaptivity is driven by the "instantaneous coefficient of variation", which is defined in [4] as the following:

$$q = \sqrt{\frac{\frac{1}{2}\left(\frac{|\nabla M|}{M}\right)^2 - \frac{1}{16}\left(\frac{\nabla^2 M}{M}\right)^2}{\left(1 + \frac{1}{4}\left(\frac{\nabla^2 M}{M}\right)\right)^2}} \qquad (13)$$

where $|\nabla M|$ is the gradient magnitude and $\nabla^2 M$ is the Laplacian operator.

Because of the common background formulation and its diffuse application for SAR images, we focus on the following in the PDE-based methods. The Lee and Frost methods and their enhanced versions are included in some specialized commercial tools for remote-sensing image processing, such as ENVI [16]. SRAD has not been included, but given its good performances, we foresee that its application will in future be a substitute for the other methods. The wavelet-based approach has been compared to the Lee and Frost approach in a previous paper [5], so it is not necessary to repeat such an analysis here. However, the quality assessment approach we are proposing here should be applied to gain quantitative evidence of the visual comparison for different filters and different applications than the ones described here.

IV. Statistical Performance Evaluation of Despeckling Filters

Image quality evaluation metrics have been described in the literature, and most are based on a noise-free image. It is the case of using simulated images, as in more recent papers, such as [26] and [29].

In the case of real data (in medical or remote sensing applications), this strategy is never possible, and the best filter is usually selected based on qualitative evaluations performed through visual analysis.

SAR images are acquired with inherent speckle noise; thus, it is important to find a metric to measure the quality of the filtered results without a noise-free image.

Regardless of the approach used to reduce the effect of the speckle noise, the ideal de-speckling method preserves radiometric information, which concerns the edges between different areas and the spatial signal variability, for example, textural information. In addition, it avoids geometrical distortions such as blocking (or blotching) artifacts. In the past, a decrease in variance without changing the mean of different sample classes, based on Shi and Ko Fung [11], was considered.

Even though the evaluation of noise removal from SAR images was historically based on a comparison between the Equivalent Number of Looks (ENL) of the filtered SAR image with respect to the original ENL, it was soon clear that such a measure is insufficient to take the various mentioned aspects into account.

Given the filtered image $F(x, y)$, the Equivalent Number of Looks (ENL) [5] is defined as follows:

$$ENL = \frac{mean(F)^2}{\text{var}(F)} = \frac{\overline{F}^2}{\sigma^2_F}. \qquad (14)$$

It is straightforward to notice that, by definition, ENL is the sample ISNR measure. It is therefore clear that the higher the ENL value for a filter, the higher the efficiency of improving the signal-to-speckle ratio over homogeneous areas will be. Because the coefficient of variation is the cost minimized by the described filters, one can also easily verify the following:

$$ENL = CV^{-2}. \qquad (15)$$

From among the statistical parameters, someone can evaluate the preservation of radiometric information, such as MSE (Mean Squared Error), RMSE (Root Mean Squared Error), and MAE (Mean Absolute Error). For noise reduction, we recall the PSNR (Peak Signal-to-Noise Ratio) and the correlation (ρ). These methods all require a noise-free image. The filter is applied to a version of the same image, which is corrupted by known simulated noise. A comparison is performed between such noisy images and the original noise-free image.

Specifically, the Mean Squared Error and the Root Mean Squared Error both measure the quality change between the original and the processed image. Whereas edge sharpness is very important for both human interpretation and automatic segmentation, it cannot be monitored by MSE [22]. The Mean Absolute Error (MAE) can be computed in the form of a Minkowski metric and is another parameter that is often considered to be more perceptually significant than the MSE [23].

Speckle suppression is sometimes evaluated in terms of fidelity by comparing the structure similarity between the filtered image and the noise-free image. A correlation-based structural similarity measure is given by the parameter, ρ, which is defined in [24] and reported in [26] and is essentially the local cross-correlation coefficient of the two images.

With respect to the preservation of edges, the Edge Preservation Index (EPI) and False Edges Index (FEI) have been proposed in the literature. EPI computes the ratio between the gradient of the filtered image and the noisy image edges [27]. Its range is [0,1], which indicates how many of the original image's edges have been preserved by processing. FEI quantifies how many edges have been artificially introduced during the filtering

process. A good de-speckling algorithm should have a high *EPI* and a reasonably low *FEI*.

In other words, as a statistical description, *EPI* represents the "sensitivity", which measures the proportion of real positive edges that are correctly identified. It is the complement of the statistical Type I error. *FEI* represents Type II error, which is inversely related to the "specificity" parameter, which measures the proportion of negatives that are correctly identified.

Finally, Pratt's Figure Of Merit (*FOM*) [28] is another index for edge preservation. It is defined as the following:

$$FOM = \frac{1}{\max\{n_d, n_r\}} \cdot \sum_{i=1}^{nd} \frac{1}{1 + \gamma d_i^2} \qquad (16)$$

where n_d is the number of detected edge pixels in the noisy image, n_r is the number of reference edge pixels in the noise-free image, and d_i is the Euclidean distance between the ith detected edge pixel and the nearest reference edge. Parameter γ is an arbitrary constant that is typically set to 0.11. *FOM* ranges between 0 and 1, with a unity value for ideal edge detection.

It is easy to notice that for the edge-preservation indexes mentioned here, results strongly depend on the algorithm used for the detection of edges, starting from the original and the filtered images. The literature reports methods that span from Roberts and Sobel to Laplacian or Canny operators [25].

A few other measures do not require simulated images, and these are of interest in the case study of SAR images. An example is the Speckle Suppression Index (*SSI*), which is typically used to evaluate the efficiency of a filter. Unfortunately, it turns out that such a measure is misleading because it does not simultaneously take into account any mean preservation measure.

V. THE PROPOSED METHOD

A. Statistical Analysis

A revised statistical approach is proposed here to discriminate the best filter for noise reduction, starting from existing methods, with the aim of obtaining a more exhaustive and significant result. Different metrics and criteria are used for the evaluation of a filter's efficiency. Only numerical parameters that do not require original noiseless images are addressed here because images are corrupted by noise when dealing with real applications.

Some parameters already presented in the literature are analyzed, such as the Speckle Suppression Index (*SSI*) [29] and the Speckle Suppression and Mean Preservation Index (*SMPI*) [30]. To solve some of the drawbacks of existing measures, two new statistical indexes are proposed, namely the Mean Preservation Index (*MPI*) and the Mean Preservation Speckle Suppression Index (*MPSSI*).

Traditionally, to evaluate the mean preservation filter ability, a simple qualitative comparison of the mean values was made in the previous literature. Because the purpose of this paper is to perform a quantitative, objective analysis, a new index is introduced that makes use of the sample mean of the original speckled image and of the filtered image, as computed from a homogeneous region.

In a homogeneous region r, the Mean Preservation Index (*MPI*) is proposed to be the following:

$$MPI = \left| \frac{\mu_{Mr} - \mu_{Fr}}{\mu_{Mr}} \right| \qquad (17)$$

where $M(x, y)$ is the generic speckled image and $F(x, y)$ is the filtered one, as defined above.

Independently on the actual image content and the RCS, it appears to be a good representative of the mean preservation capability of a filter because it is a normalized measure. This scenario allows a filter comparison that is independent from the specific SAR image acquisition mode to be made with various homogeneous regions.

When addressing the noise reduction ability of a filter, we show that some previously proposed indexes are affected by serious problems that have not always been appropriately noted.

The Speckle Suppression Index (*SSI*), which is widely used in the literature [29], [30], corresponds to the ratio between the normalized standard deviations of the image after and before filtering:

$$SSI = \frac{s_{Fr}}{\mu_{Fr}} \cdot \frac{\mu_{Mr}}{s_{Mr}}. \qquad (18)$$

It is notable that this parameter is the ratio between the *CV* of the filtered image and that of the original image; in other words, it is the ratio of the two squared-root *ENL*:

$$SSI = \frac{\sqrt{\text{var}(F)}}{mean(F)} \cdot \frac{mean(M)}{\sqrt{\text{var}(M)}}. \qquad (19)$$

Compared with the original image, a filtered image tends to have less variance because speckle is reduced. The smaller the *SSI* value is (less than one), the greater the speckle suppression. It is obvious that *ENL* and *SSI* are reliable only when the filter simultaneously has good mean-preservation properties.

To solve this last problem, the Speckle Suppression and Mean Preservation Index (*SMPI*) was proposed by Shamsoddini in [30], which is defined as follows:

$$SMPI = (1 + |\mu_{Mr} - \mu_{Fr}|) \cdot \frac{s_{Fr}}{s_{Mr}}. \qquad (20)$$

Because, in this case, the mean difference between the speckled and filtered image is not normalized, this last measure shows higher values for larger backscattering regions. To address this problem, we propose here a new index called the Mean Preservation Speckle Suppression Index (*MPSSI*), which turns out to be better normalized with respect to *SMPI* and is better for a comparison of various filters on different images:

$$MPSSI = \left| 1 - \frac{\mu_{Fr}}{\mu_{Mr}} \right| \cdot \frac{s_{Fr}}{s_{Mr}}. \qquad (21)$$

Recalling (17), we rewrite the above equation as follows:

$$MPSSI = MPI \cdot \frac{s_{Fr}}{s_{Mr}}. \qquad (22)$$

According to these two last indexes, the lower values indicate better performance of the filter in terms of the mean preservation and noise reduction, independently of the actual mean value.

B. Frequency Analysis

In this section, we address a novel approach to the evaluation of the filtering results quality, which is based on the observation that the visually perceived quality is not completely described by the classical statistical and deterministic parameters that are presented in Section V.A.

We propose to deeply investigate the behavior of non-linear filters, referring to the desired properties of good image filters. In general, the major properties of digital 2D smoothing filters are as follows [31]:

- Zero gain at zero frequency;
- Isotropic behavior;
- Higher attenuation to higher frequencies, in other words, monotonic frequency response.

These properties, which address, respectively, the mean preservation, invariance to image rotation, and ideal low-pass behavior without phase reversal, can be assessed through a specific spectral analysis of the obtained results.

In addition to the above desired features, non-linear filters address the problem of edge-preservation or enhancement, but are often subject to distortions and artifacts. It is well-known that the median filter suffers from streaking or blocking effects. This drawback has often been observed, but has never been evaluated in a quantitative way.

Therefore, our idea is to propose a numerical, objective approach that can address the mentioned aspects of the problem. To this end, we propose to analyze the changes introduced by the filter to the image spectrum. Specifically, the output energy spectrum is analyzed when a homogenously speckled region is filtered. Such a region is hereafter referred to as a "test region".

Although it is not possible to define a transfer function of a non-linear filter, we introduce the "Equivalent Transfer Function (ETF)", $H^2(k_x, k_y)$, which is defined as the ratio between the output spectrum S_{out} and the input spectrum S_{in} when we are considering a test region.

In the following specific case:

$$H^2(k_x, k_y) = ETF(k_x, k_y) = \frac{S_{out}}{S_{in}} = \frac{|\Phi_F(k_x, k_y)|^2}{|\Phi_M(k_x, k_y)|^2},$$
(23)

where $\Phi_M(k_x, k_y)$ and $\Phi_F(k_x, k_y)$ are the 2D Discrete Fourier Transform (DFT) of the speckled and filtered image, respectively. As usual, k_x and k_y are the horizontal and vertical frequencies, respectively.

Such a function represents the equivalent linear filter that should have produced the same effect on that same input image. With this relation, we can not only evaluate the smoothing effect of the filter on that specific image portion but we can also visualize and measure any distortion that arises.

A specific metric will be proposed in this paper to obtain quantitative measures of the above filtering properties. Such indexes are independent of the image type and content, as well as of the applied filter, thus providing a tool for absolute/objective evaluation, which is useful for more than the comparison of different methods.

The three properties proposed look at the distortions that are introduced into the filtered spectrum with respect to the original spectrum in a selected area of homogeneous properties. By

analogy with the linear filter characteristic analysis and referring to the first property of mean-preservation, we define the Static Power Gain as $H^2(0,0) = ETF(0,0)$. The mean-preservation filter quality is therefore related to such a power gain, which should be zero decibels for a perfectly preserving filter. It becomes obvious that such a value and the mean-preservation criteria described in Section V.A are correlated. In fact, for an image portion $M(x, y)$ of size $W_x \cdot W_y$, the 2D DFT is the following:

$$\Phi_M(k_x, k_y)$$
$$= \sum_{\nu_1=0}^{W_x-1} \sum_{\nu_2=0}^{W_y-1} M(\nu_1, \nu_2) \cdot e^{-j2\pi(k_x\nu_1/W_x)} \cdot e^{-j2\pi(k_y\nu_2/W_y)}.$$
(24)

Because the following is true:

$$\Phi_M(0,0) = \sum_{\nu_1=0}^{Wx-1} \sum_{\nu_2=0}^{Wy-1} M(\nu_1, \nu_2) = W_x \cdot W_y \cdot \mu_M \quad (25)$$

and

$$\Phi_F(0,0) = \sum_{\nu_1=0}^{Wx-1} \sum_{\nu_2=0}^{Wy-1} F(\nu_1, \nu_2) = W_x \cdot W_y \cdot \mu_F, \quad (26)$$

one can derive the following:

$$H^2(0,0) = \frac{|\Phi_F(0,0)|^2}{|\Phi_M(0,0)|^2} = \frac{\mu_F{}^2}{\mu_M{}^2}. \quad (27)$$

In other words, one can conclude that *MPI* and the Static Power Gain are functionally related by:

$$MPI = |1 - H(0,0)| = \left|1 - \sqrt{ETF(0,0)}\right|. \quad (28)$$

A good filter should be invariant to rotation, in other words, it must produce the same effect on an image and its rotated copy. As a consequence, the second desired filter property refers to the *ETF* isotropy.

A 2D function is isotropic if it has a circular symmetry; therefore, the ideal isotropic filter should have a constant value along any circle that is centered at the origin of the frequency space. For any constant value C, the solution of the system is a constant value:

$$\begin{cases} f_1(k_x, k_y) = ETF(k_x, k_y) \\ C = k_x{}^2 + k_y{}^2 \end{cases} \quad . \quad (29)$$

Alternatively, for an isotropic function, all of the *ETF* sections derived by intersecting with a vertical plane passing from the origin and having any angle with the domain space coordinates are equal. Through a transformation from Cartesian to polar coordinates, one obtains $ETF_{pol}(\rho, \theta)$.

For isotropic filters, we have the following:

$$\forall \rho_0, \forall(-\pi < \theta \leq \pi)$$
$$ETF_{pol}(\rho_0, \theta) = const$$
$$\forall(\theta_0, \theta_1), \theta_0 \neq \theta_1, \forall(0 < \rho \leq \rho_{max})$$
$$ETF_{pol}(\rho, \theta_0) = ETF_{pol}(\rho, \theta_1). \quad (30)$$

For this goal, the *ETF* values along a generic circle of the stop-band spectral domain are plotted for each filter that is considered. A constant plot for any circle radius is representative of an optimal isotropic filter. To the contrary, a non-constant value is representative of an anisotropic behavior.

When the same metric is adopted as a measure of such a property, for example a dispersion value, the proposed approach represents a procedure for a quantitative comparison from among various filters, as related to their isotropy.

As a special case, looking to the 0 and to the $\pi/2$ degree sections, the necessary (but not sufficient) isotropic condition is:

$$ETF_{pol}(\rho, 0) = ETF_{pol}\left(\rho, \frac{\pi}{2}\right) \tag{31}$$

which is equivalent to:

$$ETF(k_x, 0) = ETF(0, k_y). \tag{32}$$

To evaluate the third filter spectral property, which addresses ideal low-pass behavior, we propose the evaluation of the Stop-Band Ripple Amplitude similarly to classical linear filter analysis. We then propose to evaluate the presence and strength of the undesired sidelobes with the commonly used parameter of the Peak Sidelobe Ratio (*PSLR*) [32], which is defined as the ratio of the highest sidelobe level to the peak of the function. Another useful parameter is the Integrated Sidelobe Ratio (*ISLR*), which is defined by the ratio of the energy contained in the sidelobe to the energy contained in the main lobe of the response [32].

Quantitatively, the *PSLR* can be evaluated for each filter for comparison as follows:

$$PSLR = \frac{\max\{ETF(k_x, k_y)\}}{ETF(0, 0)} \tag{33}$$

where the max operator applies to the *ETF* and looks for the largest local maximum (excluding the mainlobe), thus referring to the highest sidelobe.

Similarly,

$$ISLR = \frac{\iint_{sidelobe} ETF(k_x, k_y)\, dk_x\, dk_y}{\iint_{Mainlobe} ETF(k_x, k_y)\, dk_x\, dk_y}. \tag{34}$$

In the definition of the highest sidelobe, we define its position in the spectral plane by defining the following:

$$(k_{x\max}, k_{y\max}) = \arg\max\{ETF(k_x, k_y)\}. \tag{35}$$

When the *ETF* is circularly symmetric, the largest sidelobe can be located by analyzing only one of its vertical sections. It follows, based on (30), that

$$\arg\max\{ETF(k_x, k_y)\} \equiv \arg\max\{ETF_{pol}(\rho, \theta_0)\} \quad \forall \theta_0. \tag{36}$$

Therefore,

$$k_{x0\max} = \arg\max\{ETF(k_x, 0)\}$$
$$k_{0y\max} = \arg\max\{ETF(0, k_y)\} \tag{37}$$

and

$$k_{x0\max} = k_{0y\max} \tag{38}$$

$$(k_{x\max}, k_{y\max}) = \left\{ (k_x, k_y) \,\middle|\, \left(k_x^2 + k_y^2 = k^2_{x0\max}\right) \right\}. \tag{39}$$

It also follows that

$$\max\{ETF(k_x, k_y)\} = \max\{ETF(k_x, 0)\}$$
$$= \max\{ETF(0, k_y)\}. \tag{40}$$

Therefore, for isotropic filters,

$$PSLR = \frac{\max\{ETF(k_x, 0)\}}{ETF(k_x, 0)|_{k_x=0}} = \frac{\max\{ETF(0, k_y)\}}{ETF(0, k_y)|_{k_y=0}}. \tag{41}$$

Additionally, from (31)–(32), one can observe the following:

$$\max\{ETF(k_x, k_y)\}$$
$$= ETF(k_{x\max}, k_{y\max}) = ETF(k_{x0\max}, 0)$$
$$= ETF_{pol}(\rho, 0)|_{\rho=k_{x0\max}}. \tag{42}$$

It then appears that the complex computation required in (32) is in fact a search for the local maxima of a single 1D plot.

In conclusion, we propose to study the 1D plots of $ETF(k_x, k_y)$ that pass from the origin in the k_x and k_y directions. With these two functions, we can gain much information about isotropy and monotonicity at the same time.

When a filter has a separable *ETF*, the following holds:

$$ETF(k_x, k_y) = ETF_x(k_x) \cdot ETF_y(k_y) \tag{43}$$

and

$$ETF(k_x, 0) = ETF_x(k_x) \cdot ETF_y(0) \tag{44}$$

and it appears that the considerations in (32) and (42) are not only necessary but also sufficient conditions for the evaluation of filter isotropy and monotonicity, respectively.

C. Proposed Method Flow

By accounting for the considerations described in Sections V.A and V.B, a general method for assessing filter performances is proposed, according to the flowchart of Fig. 1.

A generic image $M(x, y)$ is given as input to a given filter. The final aim of the process is to compute the parameters φ_1, φ_2, φ_3, and φ_4, which are useful for the filter evaluation and for the comparison with the other filters.

As already stated, the only statistical analysis is not sufficient for a comprehensive performance evaluation. Therefore, the left side of the flowchart is always completed by the right side, which is devoted to the spectral-based evaluation. From among the statistical parameters, the one parameter selected is the *MPSSI* index, which is associated with the φ_1 index. Additionally, the frequency parameters are all derived from the *ETF* function, which is computed starting from the original and the filtered images.

The three spectral indexes are the following
— φ_2, associated with the $ETF(0, 0)$ value (corresponding to the complement of *MPI*);
— φ_3, the isotropy index, computed as:

$$\forall \rho_0 \text{ in } stop-band, \forall (-\pi < \theta \le \pi)$$
$$\max_{\rho_0}\{\max_{\theta}\{ETF_{pol}(\rho_0, \theta)\}\}$$
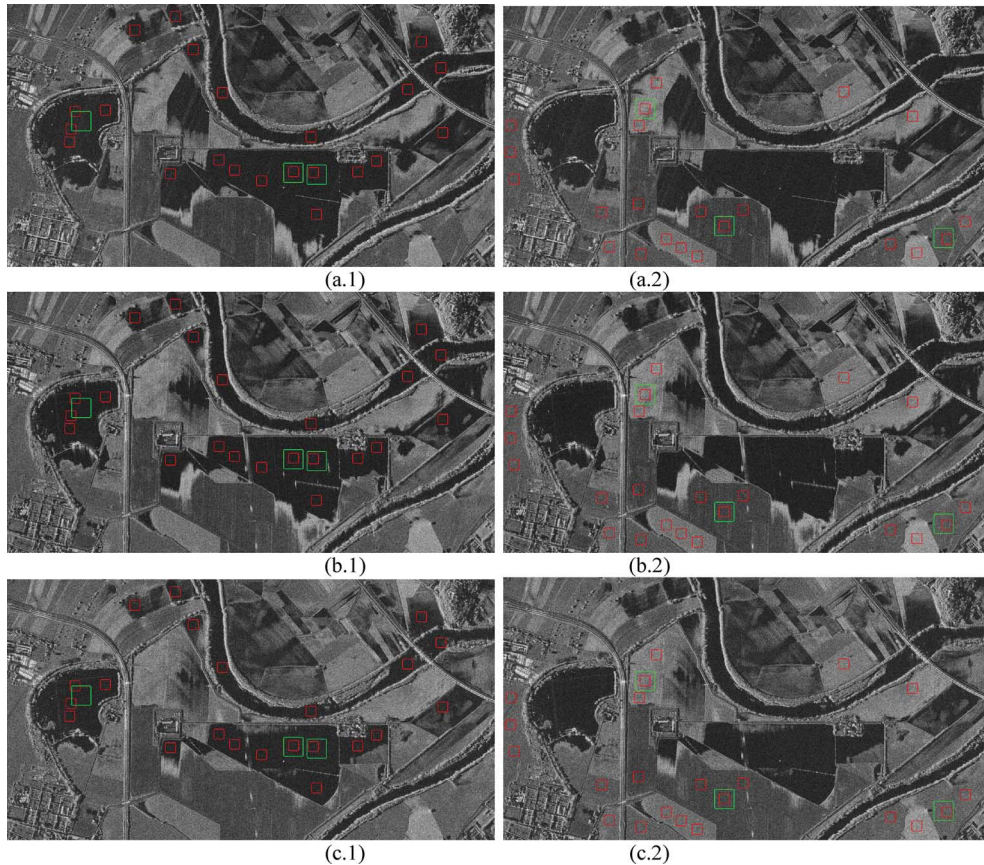
Fig. 2. Cosmo/Skymed images (after an appropriate histogram stretching) acquired in Spotlight mode (a.x) on April 29th, (b.x) on April 30th and (c.x) on May 1st. Red samples are used for statistical analysis, and green samples are used for frequency analysis of "Class 1" (x.1) and "Class 2" (x.2).
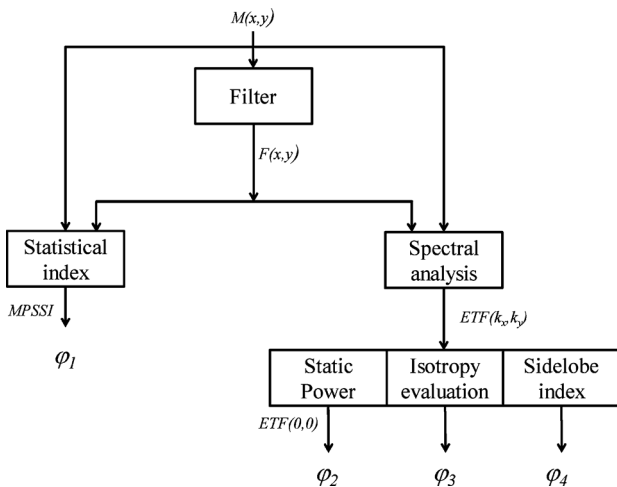
Fig. 1. Flowchart of the general method for assessing filter performances.

— φ_4, the sidelobe index, given by the *PSLR*.

With such parameter computations, a good filter (which addresses the specific image $M(x, y)$) is characterized by low φ_1, high φ_2, low φ_3, and low φ_4 values. In the comparison of the various filters, if one method verifies all of the criteria, then it must be selected as the best method. Otherwise, if various criteria are satisfied by various filters, the selection of the best filter is determined by weighting the relevance of the single index.

The major difference with the performance evaluations methods existing in the literature lies in the fact that specific spectral analysis indexes are proposed in addition to the classical statistical analyses. To make it possible to perform such a spectral analysis of non-linear filters, we must use the proposed *ETF* definition, which relates each filtered image with its original version, thus judging the filter performance as related to that specific image. In addition, the statistical indexes proposed here are better designed to provide appropriate evaluations of the speckle suppression property, allowing for a direct comparison from among filters.

VI. EXPERIMENTAL RESULTS

A. Dataset

In this study, experiments were performed on various Cosmo-Skymed SAR images (X-band) that were acquired in different acquisition modes. The results presented here refer to three Spotlight images named T1, T2, and T3 (1-meter resolution), which are shown in Fig. 2. These images cover a geographical area of 5.4 km^2. A Stripmap pair (2.5 meters resolution) of images (named T4 and T5) is represented in Fig. 3 (these images correspond to an entire frame, approximately $2,575 \text{ km}^2$). The Spotlight images were acquired on April 29th (image T1), April 30th (image T2) and May 1st (image T3), 2009, in different flight configurations, whereas the Stripmap image pair, in the ascending/right configuration, was acquired
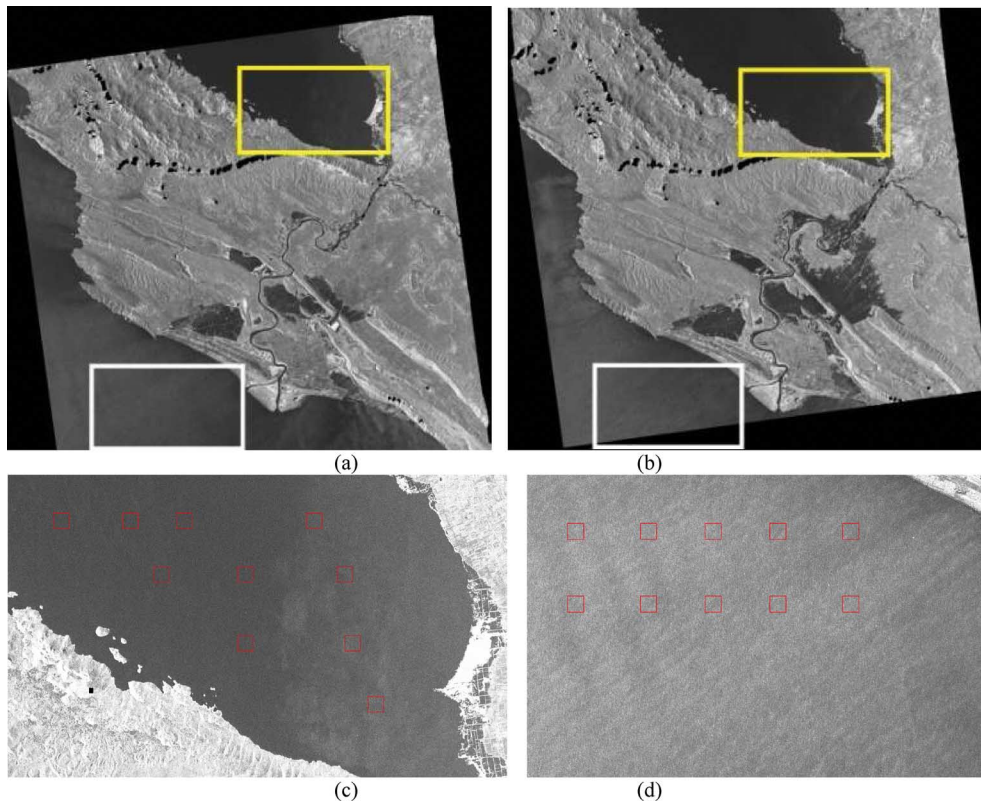
Fig. 3. Cosmo/Skymed images (after appropriate histogram stretching) acquired in Stripmap mode on January 16th (a) and 24th (b). In yellow and white, the area of "Class 1" and "Class 2", respectively. The details of samples used for statistical analysis of "Class 1" (c) and "Class 2" (d). (These images correspond to an entire frame, covering an area of approximately 2,575 km^2).

TABLE I
ACQUISITION PARAMETERS CONFIGURATION. ID: IDENTIFICATION; DATE:
ACQUISITION DATE; TIME: ACQUISITION DATA TIME; A: ACQUISITION
MODE (SP = Spotlight, ST = Stripmap); P: POLARIZATION;
O: ORBIT DIRECTION (D = Descending, A = Ascending);
L: LOOK ANGLE (L = Left, R = Right)

ID	Date	Time	A	P	O	L
T1	29/04/09	18:46	SP	HH	D	L
T2	30/04/09	05:32	SP	HH	A	R
T3	01/05/09	05:32	SP	HH	A	R
T4	16/01/10	04:45	ST	HH	A	R
T5	24/01/10	04:45	ST	HH	A	R

on January 16th and 24th, 2010. The geometric acquisition parameters are shown in Table I.

The Spotlight images show an area of North Italy, and the Stripmap images show the Shkodër area in Albania; both refer to the monitoring of flooding events and were acquired in the context of the OPERA project [33].

The Spotlight and Stripmap COSMO products used are Geocoded Ellipsoid Corrected (GEC)_B single-look Amplitude images [21]. It was not necessary to calibrate the images to assess the performance of the filters.

As a test set for the statistically based performance evaluation, some homogeneous regions have been manually selected from the two datasets. From the Spotlight images, 22 samples in every image for Class 1 have been selected, as shown in red in Figs. 2(a.1), 2(b.1), and 2(c.1). The 22 samples for Class 2 are shown in red in Figs. 2(a.2), 2(b.2), and 2(c.2). Each sample

covers a 61×61 pixel wide area. From the Stripmap images, 10 samples from the image pair have been analyzed, both for Class 1 and for Class 2, always covering an area of 61×61 pixels, as shown in Fig. 3(c) and (d), respectively.

For both datasets, Class 1 test regions correspond to calm water areas, which are characterized by low backscattering and low speckle values. Class 2 regions correspond to heterogeneous no-water areas in Spotlight images. In the Stripmap image pair, Class 2 test regions have been chosen in the sea area, but the characteristics are different with respect to calm water because of some wind, which increases backscattering and speckle. Thus, different classes have been chosen to prove the effectiveness of the evaluation method and its applicability to any image type.

Because of the need for larger regions for frequency analysis, in Spotlight images test samples that are 121×121 pixels wide are analyzed. In Fig. 2, such test regions are noted in green. The regions selected for the frequency analysis of the Stripmap images are in the same location as the red regions in Fig. 3(c) and (d), but have a larger size (201×201 pixels).

Each filter chosen for the comparison requires the setting of parameters and thresholds, such as the size of the window neighborhood (d), a normalization constant (k), the number of iterations (N) and the time step (t). In some cases, the manual delineation of a homogenous area is required. In such cases, H represents the area size.

Specifically, only one configuration has been selected, setting each filter parameter at a predefined value, except

TABLE II
FILTER PARAMETERS CONFIGURATION. L = Lee; F = Frost; EL = Enhanced Lee; EF = Enhanced Frost; $S8$ AND $S200$ = SRAD WITH DIFFERENT PARAMETERS. $\times$ = Requested Parameter; $/$ = Not Requested Parameter

	d	k	H	N	t
L	7	–	$\times$	–	–
F	7	1	$/$	–	–
EL	7	1	$\times$	–	–
EF	7	1	$\times$	–	–
$S8$	–	–	$/$	8	0.5
$S200$	–	–	$/$	200	0.01
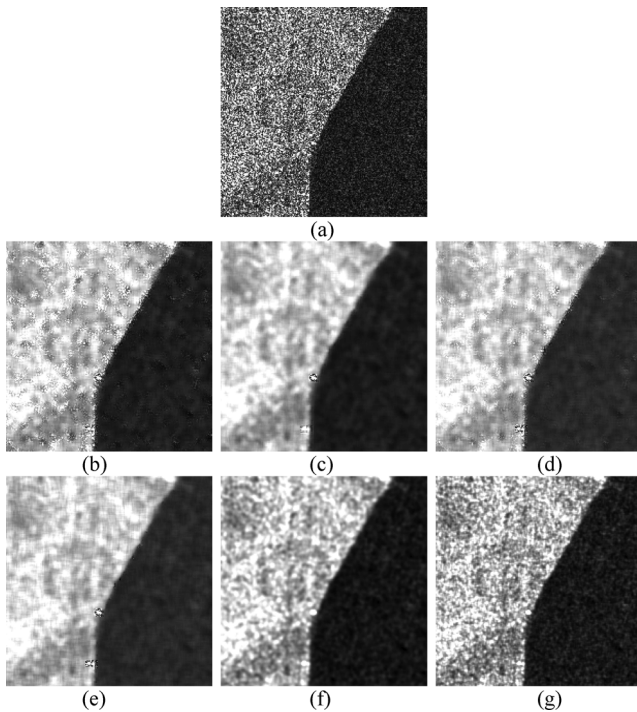
Fig. 4. (a) Sample of an original CSK image acquired in Spotlight mode. Result by (b) Lee filter; (c) Frost filter; (d) Enhanced Lee filter; (e) Enhanced Frost filter; (f) SRAD filter with parameter 8–0.5 (SRAD-8); (g) SRAD filter with parameter 200–0.01 (SRAD-200).

for the SRAD filter, for which the results are referred to two settings. When the filter requires the H parameter, a homogenous area belonging to a water area that corresponds to 0.01% of the total image size has been selected. The parameter configurations chosen for the filters comparison are reported in Table II.

B. Filters

A visual analysis is presented in Fig. 4, where a specific area of an original image is reported, with the corresponding filtered versions. It refers to an original Cosmo/Skymed image that was acquired in Spotlight mode depicting a boundary zone between fields and water. As can be seen, the Frost and the Enhanced Frost filters introduce significant blocking effects, although less than the Lee and the Enhanced Lee filters. Both SRAD versions do not show these artifacts and better preserve the details and edges. Note that the SRAD-8 appears to achieve a better noise

reduction compared with SRAD-200. Then, from a visual inspection, SRAD despeckled images more closely resemble the original image when compared to the others.

C. Statistical Analysis

For the classical statistical analysis, the mean and standard deviation of the original (noisy) images and of the corresponding filtered images have been computed for each test region. The averaged region values are summarized in Tables III and IV. One can notice that, as expected, the *ISNR* value for the original Spotlight images (T1, T2 and T3) is equal to 3.6 in both classes.

As described above, a good filter approach preserves the mean value of the original image while it decreases the standard deviation value. From Tables III and IV, one can observe that all of the filters preserve the mean and reduce the standard deviation. Specifically, SRAD and Frost filters retain the mean better compared with the other filters. The best reduction in the standard deviation is always obtained by the Frost algorithm. The analysis shows that the filter performances are independent of the sample classes because both classes exhibit the same behavior in statistical terms, proving good robustness when addressing the mean preservation and standard deviation decrease.

As already described, the classical mean-preservation indexes do not coincide with human perception. In fact, from a visual inspection of Fig. 4, SRAD despeckled images more closely resemble the original image when compared to the others.

Starting from these values, it is possible to compute the various statistical indexes that are presented in Section V.A. First, we consider the Mean Preservation Index (*MPI*). This index uses the sample mean of the original (noisy) and filtered images: the best filter presents a low value. Graphs in Figs. 5 and 6 report the obtained *MPI* values as computed by averaging the *MPI* on the test regions of each class.

One can notice that SRAD-8 reaches the best performances, in terms of the minimum *MPI*, when applied to Spotlight images. In fact, the *MPI* values are approximately zero in T1, T2, and T3 images, both for "Class 1" and "Class 2". Worse results are obtained in the case of Stripmap images, where the *MPI* index presents slight changes with the variation of the filtering method, and it is impossible to identify the best filter.

While *MPI* takes into account only the mean of the original and filtered images, the Speckle Suppression Index (*SSI*) considers also the standard deviation. We can select the best filter for despeckling when the *SSI* index presents a small value. The results obtained from Spotlight and Stripmap images are illustrated in Fig. 7.

When passing from the Spotlight to the Stripmap images, the behavior of *SSI* does not change significantly with both class and image. When we considered Spotlight images we notice that the Frost filter seems to be the best filter, and the Lee and SRAD filters have a similar *SSI* value. Although the standard deviation achieved by the two filters is of the same order, the Lee filter has a bad mean-preservation behavior. This fact is not appropriately

TABLE III
MEAN VALUES ON TEST SAMPLES FROM THE T1, T2, AND T3 IMAGES. MEAN AND STANDARD DEVIATION OF "CLASS 1" AND "CLASS 2"

| | "Class 1" | | | | | | "Class 2" | | | | | |
| | Mean | | | Standard deviation | | | Mean | | | Standard deviation | | |
	T1	T2	T3	T1	T2	T3	T1	T2	T3	T1	T2	T3
Original images	18.039	27.29	37.298	9.544	14.327	19.414	47.205	77.663	86.338	25.116	40.660	45.156
Lee	17.544	26.815	36.796	2.333	3.314	4.349	46.686	77.162	85.835	6.620	9.867	10.225
Frost	17.538	26.806	36.788	1.691	2.366	3.346	46.672	77.156	85.809	5.027	7.634	7.914
Enh. Lee	17.545	26.820	36.801	1.928	2.758	3.753	46.690	77.167	85.838	5.612	8.477	8.811
Enh. Frost	17.546	26.820	36.805	1.775	2.511	3.529	46.693	77.166	85.837	5.235	7.994	8.313
SRAD-8	18.041	27.307	37.303	2.375	3.415	4.750	47.194	77.660	86.331	6.845	10.623	11.289
SRAD-200	17.541	26.802	36.797	3.441	5.053	6.914	46.697	77.157	85.830	9.653	15.190	16.468

TABLE IV
MEAN VALUES ON TEST SAMPLES FROM THE T4 AND T5 IMAGES. MEAN AND STANDARD DEVIATION OF "CLASS 1" AND "CLASS 2"

| | "Class 1" | | | | "Class 2" | | | |
| | Mean | | Standard deviation | | Mean | | Standard deviation | |
	T4	T5	T4	T5	T4	T5	T4	T5
Original images	70.052	63.497	20.800	21.991	195.288	165.428	51.788	43.757
Lee	69.589	63.107	11.246	14.331	194.556	164.839	22.574	18.313
Frost	69.811	63.358	9.138	11.790	194.761	164.951	17.363	14.035
Enh. Lee	69.665	63.222	9.714	13.249	194.700	164.920	19.272	15.646
Enh. Frost	69.688	63.259	9.571	13.072	194.726	164.936	19.011	15.434
SRAD-8	69.732	63.319	10.958	13.034	194.750	164.946	23.066	19.034
SRAD-200	69.609	63.128	13.892	15.718	194.771	164.948	32.322	27.089

described by *SSI*. Instead, in the case of Stripmap images, the traditional filters present the best results.

The final indexes investigated for the statistical analysis are the Speckle Suppression and Mean Preservation Index (*SMPI*) and the Mean Preservation Speckle Suppression Index (*MPSSI*). As presented before, both indexes must be as small as possible to determine the best filter. Figs. 8 and 9 present the results of *SMPI*, which are obtained for both types of images that were investigated, while Figs. 10 and 11 present *MPSSI* results.

In the case of Spotlight images, SRAD-8 performs the best results in terms of *SMPI* and *MPSSI*. In fact, both indexes are the lowest compared to other filters for both classes. Specifically, the *MPSSI* index is approximately zero. Instead of Stripmap images, it is not possible to select the best filter.

In conclusion, the results show that the statistical analysis method is not always able to select the best despeckling filter, mainly when addressing various acquisition parameters and classes of interest. Specifically, we found more problems in Stripmap images then an appropriate frequency analysis was applied, as originally proposed in the previous sections.

D. Frequency Analysis

Because of the inability to always select the best filter through statistical analysis, the frequency analysis proposed in Section V.B has been applied, to evaluate spectral features of filtered images.

Starting from a Class 1 region from one of the Spotlight images, Fig. 12(a) shows the DFT of the original sample and the *ETFs* as derived by (23), after the application of the filters. One can visually appreciate how the low pass effect is evident for all of the filters. However, the strong anisotropy and the geometrical distortions introduced are visible in the lateral lobes of the *ETFs*, except for the SRAD-8 and SRAD-200.

With regard to the first of the parameters that were introduced in Section V.B, the so-called Static Power Gain, $ETF(0,0)$, of "Class 1" and "Class 2" samples from Spotlight and Stripmap images are reported in the graphs depicted in Fig. 13, which describe the mean-preservation properties of each filter. It is confirmed here that the SRAD filter is the best filter in the mean preservation for Spotlight images, in accordance with the *MPI* index (see Fig. 5). It is important to note how this property is equally verified for "Class 1" and "Class
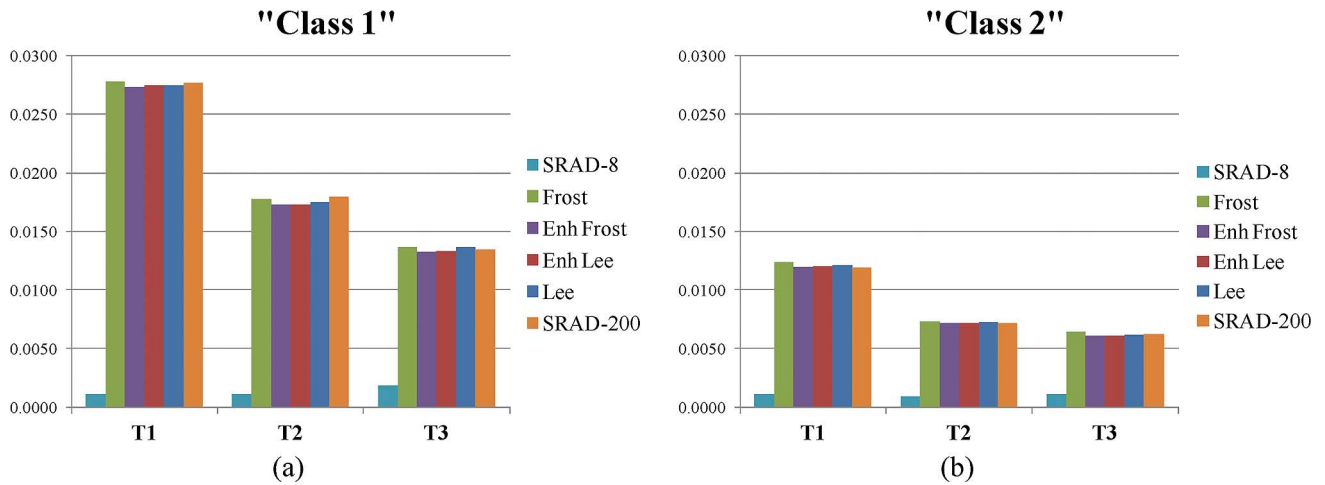
Fig. 5.   Mean Preservation Index for Spotlight images. (a) "Class 1" and (b) "Class 2".
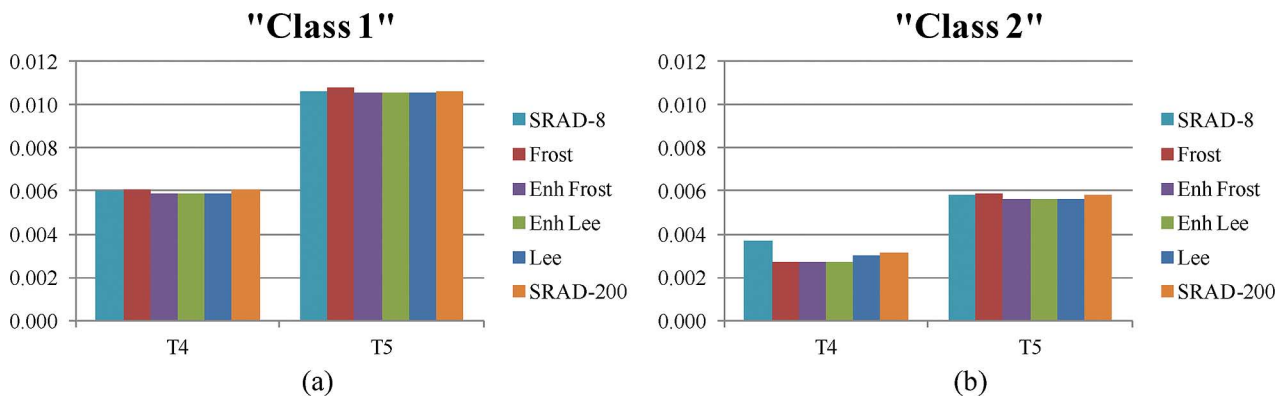
Fig. 6.   Mean Preservation Index for Stripmap images. (a) "Class 1" and (b) "Class 2".
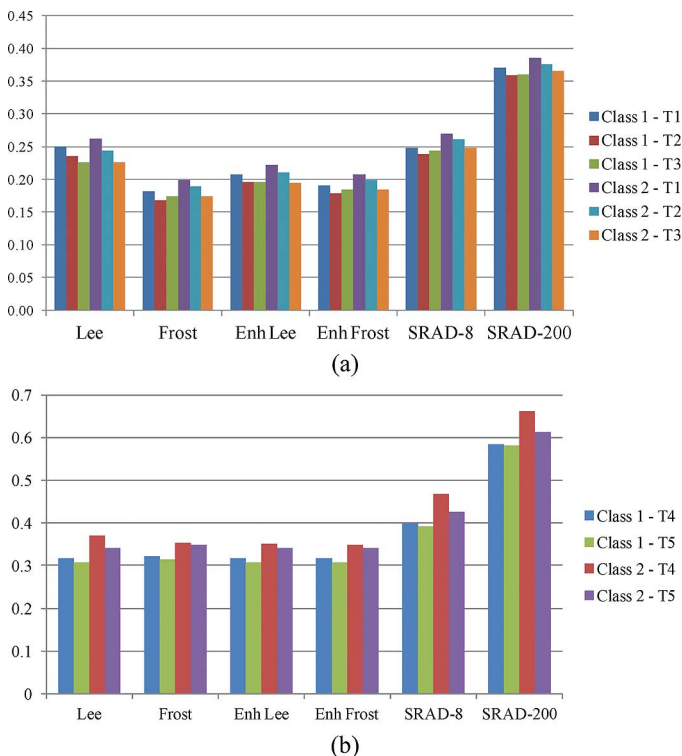
Fig. 7.   Speckle Suppression Index for the (a) Spotlight and (b) Stripmap images. The graphs show the behavior of the filtering with the class and image changing.

2", suggesting that its good performances are not affected by the image average power.

In the case of Stripmap images, the behavior of the filters related to the mean preservation is almost the same. All of the filters present the same trend for both classes; the differences among the filters and for image changes are not very significant, as concluded from the *MPI* values of Fig. 6.

The method proposed for the isotropic analysis consists of the study of the *ETFs* along the circumferences centered in the origin of the frequency axes. As an example, the plots presented in Fig. 14 show the *ETF* intensity along a fixed circle with a 40 pixel radius, $ETF_{pol}(40, \theta)$, for all of the applied filters.

As stated previously, a constant plot indicates a good isotropic effect. To this end, the plot dispersion is evaluated. From Fig. 13, one can appreciate how the plot of the Frost filter appears better than the Lee and the enhanced filters, as evident in Fig. 11. On the whole, SRAD filters show a good plot, thus confirming the visual analysis that appreciates the lower distortions introduced in the result. However, because of the larger frequency of filter SRAD200, the plot actually represents the anisotropy in the filter pass-band.

To numerically evaluate one-filter anisotropy, a complete analysis takes into account all of the circle radius that correspond to the filter stop-band. The maximum value from among these dispersions is a good parameter for describing the filter anisotropy.
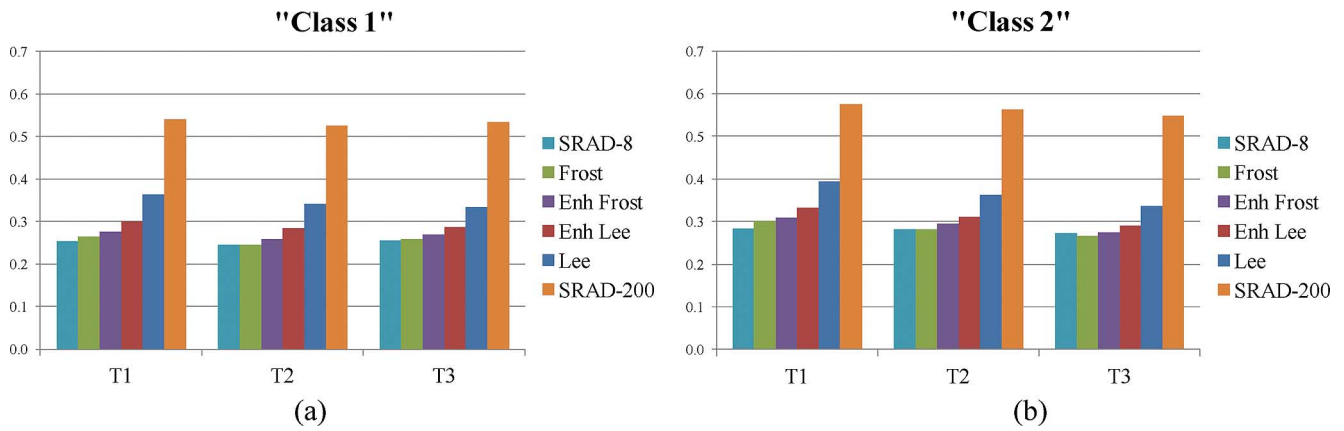
Fig. 8. *SMPI* for Spotlight images. (a) "Class 1" and (b) "Class 2". Each value is averaged over samples.
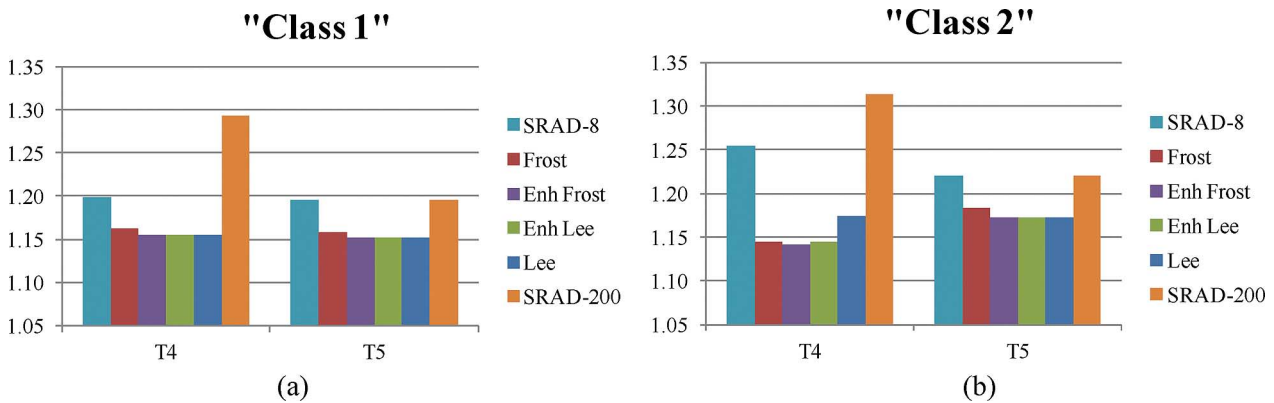
Fig. 9. *SMPI* for Stripmap images. (a) "Class 1" and (b) "Class 2". Each value is averaged over samples.
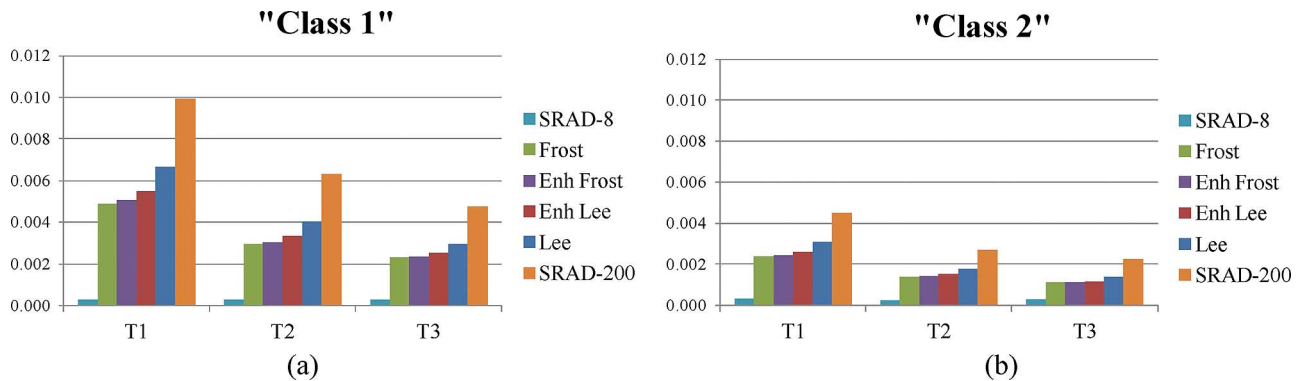
Fig. 10. *MPSSI* for Spotlight images. (a) "Class 1" and (b) "Class 2". Each value is averaged over samples.

TABLE V
MAXIMUM DISPERSION VALUES FOR POLAR *ETF* PLOTS
WITH THE CORRESPONDING RADIUS

		Max dispersion
Srad8	$ETF_{pol}(40,\theta)$	0.3535
Frost	$ETF_{pol}(35,\theta)$	0.4831
Enh_Frost	$ETF_{pol}(35,\theta)$	0.7247
Enh_Lee	$ETF_{pol}(55,\theta)$	0.6044
Lee	$ETF_{pol}(55,\theta)$	1.2140
Srad200	$ETF_{pol}(55,\theta)$	0.3776

Table V reports the maximum dispersion values for each filter, as computed for a "Class 2" region. As expected, by

excluding SRAD filters, the best effect is that achieved by Frost filters, while the Lee filter is the worst.

Thanks to the stationarity of the test regions belonging to the same class, given an image acquisition mode, the *ETFs* obtained from each region of a class have been averaged for the evaluation of the isotropy and the low-pass effect of each filter. When the *ETFs* of the Class 1 samples acquired in T1, T2, T3 Spotlight images are averaged, a unique $ETF(k_x, k_y)$ for each filter is obtained. Similarly, corresponding information for the Spotlight Class 2 test regions have been averaged. The same holds for Stripmap images: with a change of the filter applied to the original images T4 and T5, the average *ETFs* for "Class 1" and "Class 2" have been computed.
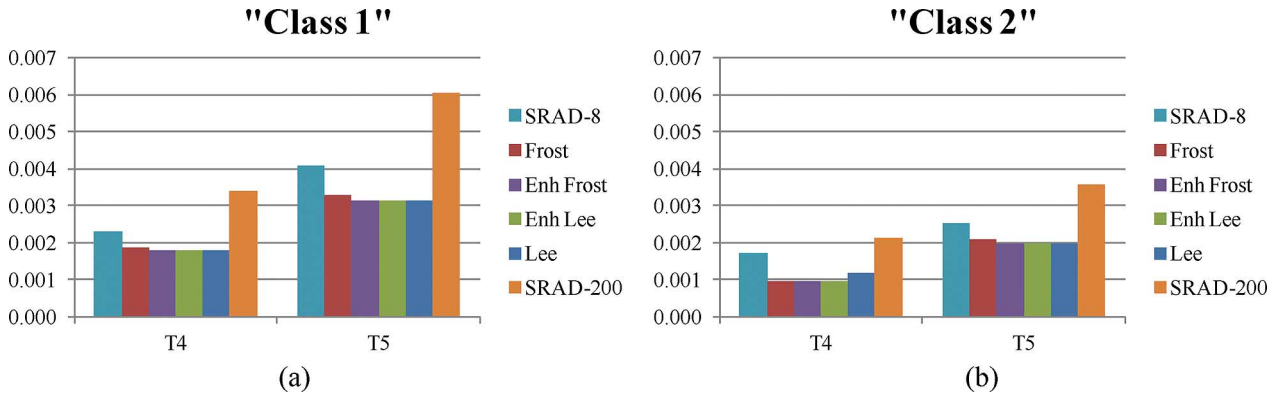
Fig. 11. *MPSSI* for Stripmap images. (a) "Class 1" and (b) "Class 2". Each value is averaged over samples.
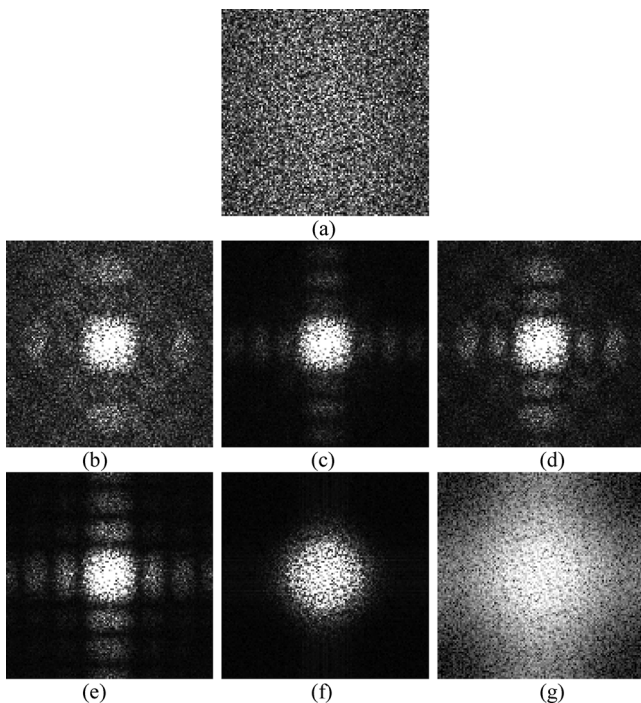
Fig. 12. Frequency analysis of a "Class 1" region from an original CSK image acquired in Spotlight mode. (a) DFT of the region; *ETF*s of the (b) Lee filtered; (c) Frost filtered; (d) Enhanced Lee filtered; (e) Enhanced Frost filtered; (f) SRAD filtered with parameter 8–0.5 (SRAD-8); (g) SRAD filtered with parameter 200–0.01 (SRAD-200).

Fig. 13. Analysis of zero frequency gain. Static power gain $ETF(0,0)$ of "Class 1" and "Class 2" samples of (a) Spotlight and (b) Stripmap images.

As suggested in Section V.B, 1D plots of $ETF(k_x, k_y)$ passing from the origin in the k_x and k_y directions, i.e., the $ETF(k_x, 0)$ and $ETF(0, k_y)$, are shown in Fig. 15. These plots refer to Spotlight Class-1 regions (Fig. 15(a) and (c)) and Spotlight Class-2 regions (Fig. 15(b) and (d)).

With this approach, one can gain a preliminary idea about the sidelobes and about the eventual anisotropy at the same time. It is possible to observe from the graphical analysis that for both classes, the traditional filters (Lee, Frost, Enhanced Lee and Enhanced Frost) do not present monotonic behavior along both the k_x and k_y directions. In contrast, both of the SRAD filters (SRAD-8 and SRAD-200) show a monotonic non-increasing trend. This aspect is especially evident in Fig. 15 because the traditional filters introduce high peaks far from the origin. The various sidelobe features of the classical filters might be computed for their comparison but do not compare with the SRAD filter. Because of the evident lack of lateral sidelobes in the SRAD plots, the related *PSLR*s have a value of zero. A direct comparison of SRAD filters with respect to the other filters is straightforward.

VII. Conclusions

In this paper, a new method for the quality assessment of despeckled SAR images has been presented. Many statistical indexes have been presented in the past for evaluating filter quality, and most of them require a noise-free image. Typically, the statistical analysis can be achieved for simulated images, but it is impossible to apply in a real context, where only noisy-images are available.
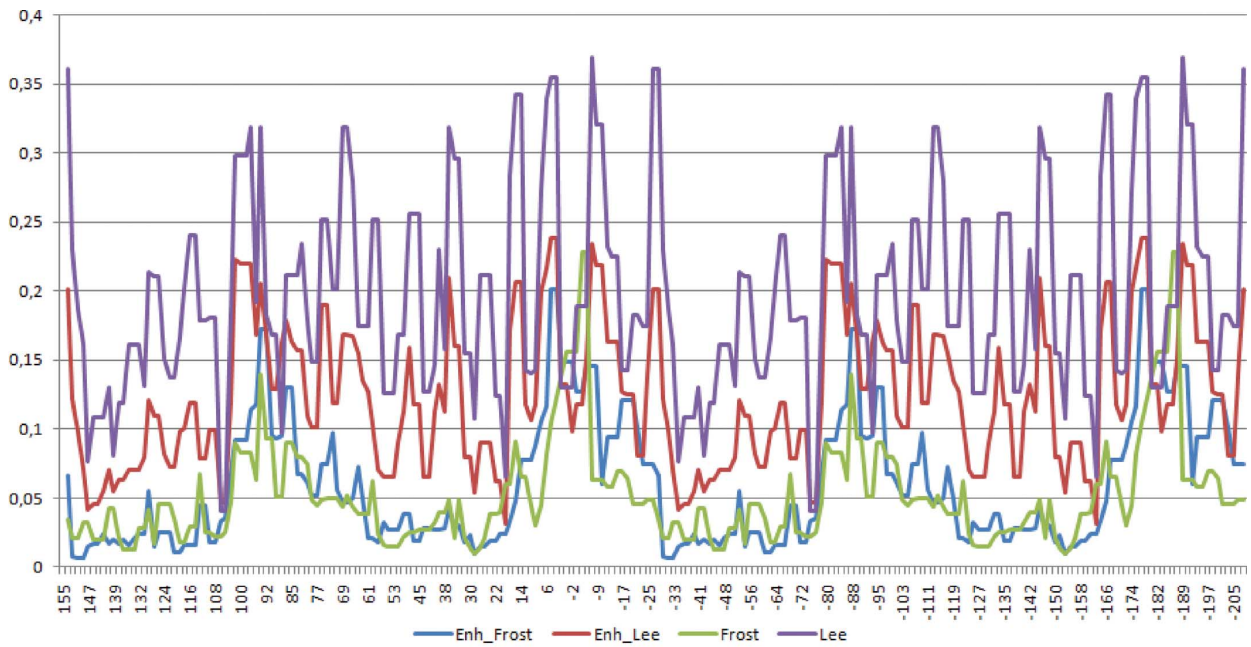
(a)
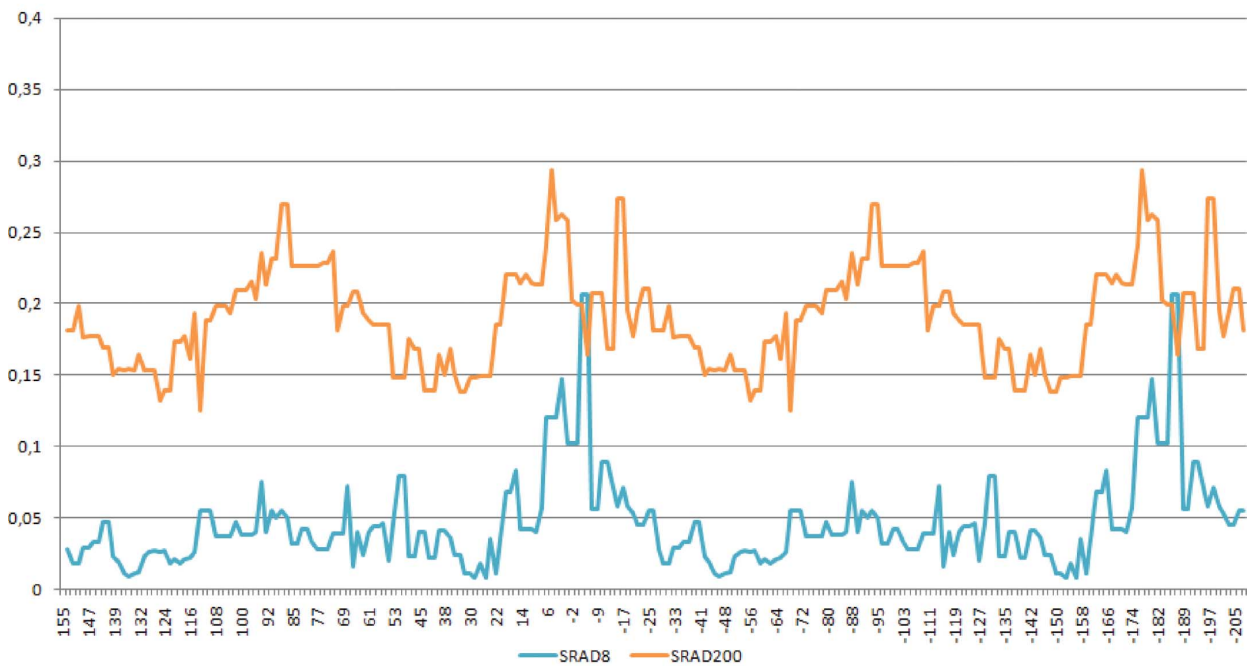
(b)

Fig. 14. Filtered circular *ETF* plot (40 pixels radius) referring to "Class 2" Spotlight region.

To counter this problem, a few indexes that do not require free-noise images have been proposed in the literature, the most common example being the *SSI* index.

Despite this fact, statistical analysis is not always able to effectively evaluate filter performances and to select the best method for despeckling filters.

To address this limitation, the present paper proposes a new approach that performs a quantitative analysis in the frequency domain. The effects of some despeckling filters on the image spectrum have been analyzed.

The performances of some of the traditional filters, such as Lee, Frost, Enhanced Lee and Enhanced Frost, are investigated, in addition to SRAD, a more recent filter that is based on anisotropic diffusion. Visual interpretation of the filtered images demonstrates that the SRAD filter achieves the best results with respect to traditional filters. Indeed, the SRAD filter not only reduces the noise without damaging the edges and textures but also does not introduce artifacts, as with traditional filters.

To obtain the same results with quantitative analysis, both statistical and frequency analysis are proposed and have been per-
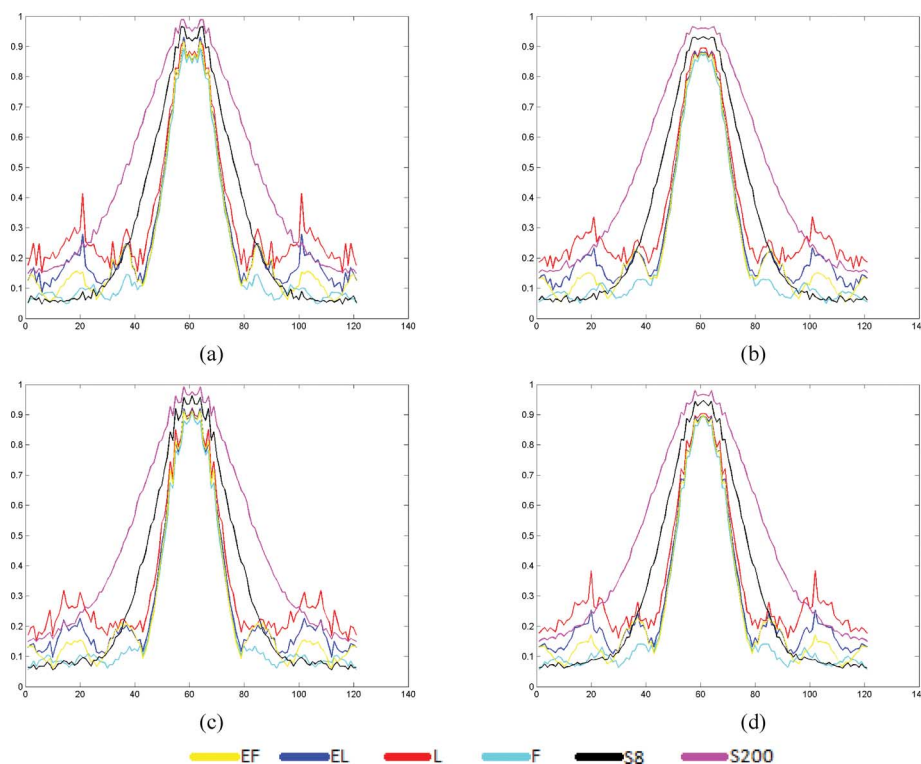
Fig. 15. *ETF* analysis along a direction. Spotlight images T1, T2, T3. $ETF(0, k_y)$ for (a) "Class 1" and (b) "Class 2". $ETF(k_x, 0)$ for (c) "Class 1" and (d) "Class 2".

formed on real SAR images. In addressing the former statistical evaluation, only indexes that do not require free-noise images have been considered because we used only real images for the experimental section. This type of analysis allows us to obtain some results, but not always the best filter can be objectively identified.

The latter analysis investigates the filtered image behavior in the frequency domain. Different values have been evaluated for the analysis of the mean preservation, the isotropy and the ideal low-pass behavior. More specifically, because of the two last measures, it is possible to prove that SRAD filters produce the best results compared with traditional filters.

Experiments on real data that were acquired through the new mission, Cosmo/Skymed, have been realized, and images were acquired in different acquisition modes (Spotlight and Stripmap), with different acquisition parameters.

The proposed methods are used here for the comparison of filters based on anisotropic diffusion, but they can easily be extended to other despeckling filters, such as filters based on wavelet transforms.

REFERENCES

[1] R. Vaccaro, P. C. Smits, and S. G. Dellepiane, "Exploiting spatial correlation features for SAR image analysis," *IEEE Trans. Geosci. Remote Sens. E*, vol. 38, no. 3, pp. 1212–1223, May 2000.

[2] P. C. Smits and S. G. Dellepiane, "Discontinuity-adaptive Markov random field model for the segmentation of intensity SAR images," *IEEE Trans. Geosci. Remote Sens. E*, vol. 37, no. 1, pp. 627–632, Jan. 1999.

[3] S. Dellepiane and E. Angiati, "A new method for cross-normalization and multitemporal visualization of SAR images for the detection of flooded areas," *IEEE Trans. Geosci. Remote Sens. E*, vol. 50, no. 7, pt. 2, pp. 2765–2779, 2012.

[4] Y. Yu and S. T. Acton, "Speckle reducing anisotropic diffusion," *IEEE Trans. Image Process.*, vol. 11, no. 11, pp. 1260–1270, 2002.

[5] L. Gagnon and A. Jouan, "Speckle filtering of SAR images – A comparative study between complex-wavelet based and standard filters," in *Proc. SPIE Int. Conf.*, 1997, vol. 3169, pp. 80–91.

[6] F. W. Ulaby, R. K. Moore, and A. K. Fung, *Microwave Remote Sensing: Active and Passive. Volume 2 – Radar Remote Sensing and Surface Scattering and Emission Theory*. Boston, MA, USA: Addison-Wesley, 1982.

[7] G. Franceschetti and R. Lanari, *Synthetic Aperture Radar Processing Techniques*. Boca Raton, Fla, USA: CRC Press, 1999.

[8] J. S. Lee, "Speckle analysis and smoothing of synthetic aperture radar images," *IEEE Trans. Comput. Graph. Image Process.*, vol. 17, pp. 24–32, 1981.

[9] J. S. Lee, "A simple speckle smoothing algorithm for synthetic aperture radar image," *IEEE Trans. Syst., Man, Cybern.*, vol. 13, no. 1, pp. 85–89, 1983.

[10] V. S. Frost, "A model for radar images and its application to adaptive digital filtering of multiplicative noise," *IEEE Trans. Pattern Anal. Mach. Intell.*, vol. 4, no. 2, pp. 157–166, Mar. 1982.

[11] Z. Shi and K. B. Fung, "A comparison of Digital Speckle Filters," in *IGARSS 1994, IEEE Int. Geosci. Remote Sensing Symp.*, Canada, Aug. 8–12, 1994, pp. 2129–2133.

[12] M. I. H. Bhuiyan, M. O. Ahmad, and M. N. S. Swamy, "New spatially adaptive wavelet-based method for the despeckling of medical ultrasound images," in *IEEE Int. Symp. Circuits Syst.*, May 2007, pp. 2347–2350.

[13] Y. Yue, M. M. Croitoru, J. B. Zwischenberger, and J. W. Clark, "Nonlinear multiscale wavelet diffusion for speckle suppression and edge enhancement in ultrasound images," *IEEE Trans. Med. Imag.*, vol. 25, no. 3, pp. 297–311, 2006.

[14] W. A. Hendricks and K. W. Robey, "The sampling distribution of the coefficient of variation," *Ann. Math. Statist.*, vol. 7, no. 3, pp. 129–132, 1936.

[15] P. Perona and J. Malik, "Scale space and edge detection using anisotropic diffusion," *IEEE Trans. Pattern Anal. Machine Intell.*, vol. 12, pp. 629–639, 1990.

[16] ENVI. [Online]. Available: http://www.ittvis.com/ProductServices/ENVI.aspx

[17] P. C. Tay, "Ultrasound despeckling for contrast enhancement," *IEEE Trans. Image Process.*, vol. 17, no. 7, pp. 1847–1860, Jul. 2010.

[18] A. Pižurica, W. Philips, I. Lemahieu, and M. Acheroy, "A versatile wavelet domain noise filtration technique for medical imaging," *IEEE Trans. Med. Imag.*, vol. 22, no. 3, pp. 323–331, 2003.

[19] S. Gupta, L. Kaur, R. C. Chauhan, and S. C. Saxena, "A versatile technique for visual enhancement of medical ultrasound images," *Digital Signal Processing*, vol. 17, pp. 542–560, 2007.

[20] M. Lysaker, A. Lundervold, and X.-C. Tai, "Noise removal using fourth-order partial differential equation with applications to medical magnetic resonance images in space and time," *IEEE Trans. Image Process.*, vol. 12, no. 12, pp. 1579–1590, Dec. 2003.

[21] COSMO [Online]. Available: http://www.e-geos.it/products/pdf/COSMO-SkyMed-Image_Calibration.pdf

[22] M. H. DeGroot, *Probability and Statistics*, 2nd ed. Boston, MA, USA: Addison-Wesley, 1980.

[23] C. J. Willmott and K. Matsuura, "Advantages of the mean absolute error (MAE) over the root mean square error (RMSE) in assessing average model performance," *Climate Res.*, vol. 30, pp. 79–82, 2005.

[24] F. Sattar, L. Floreby, G. Salomonsson, and B. Lovstrom, "Image enhancement based on a nonlinear multiscale method," *IEEE Trans. Image Process.*, vol. 6, no. 6, pp. 888–895, Jun. 1997.

[25] L. G. Shapiro and G. C. Stockman, *Computer Vision*, 1st ed. Englewood Cliffs, NJ, USA: Prentice Hall, 2001.

[26] Z. Wang, A. C. Bovik, H. R. Sheikh, and E. P. Simoncelli, "Image quality assessment: From error visibility to structural similarity," *IEEE Trans. Image Process.*, vol. 13, no. 4, pp. 600–612, Apr. 2004.

[27] H. Chunming, G. Huadong, and W. Changlin, "Edge preservation evaluation of digital speckle filters," in *IGARSS 2002, IEEE Int. Geosci. Remote Sensing Symp.*, Jun. 2002, vol. 4, pp. 2471–2473, 24-28.

[28] W. K. Pratt, *Digital Image Processing*. New York, NY, USA: Wiley, 1977.

[29] Y. Sheng and Z. G. Xia, "A comprehensive evaluation of filters for radar speckle suppression," in *IGARSS 1996, IEEE Int. Geosci. Remote Sensing Symp.*, May 27–31, 1996, pp. 1559–1561.

[30] A. Shamsoddini and J. C. Trinder, "Image texture preservation in speckle noise suppression," in *ISPRS Commission VII Symp.*, Vienna, Austria, Jul. 5–7, 2010, pp. 239–244.

[31] B. Jahne, *Digital Image Processing – Concepts, Algorithms, and Scientific Applications*. Berlin Heidelberg: Springer-Verlag, 1997.

[32] A. Freeman, "SAR calibration: An overview," *IEEE Trans. Geosci. Remote Sens.*, vol. 30, no. 6, pp. 1107–1121, 1992.

[33] S. B. Serpico, S. Dellepiane, G. Boni, G. Moser, E. Angiati, and R. Rudari, "Information extraction from remote sensing images for flood monitoring and damage evaluation," *Proc. IEEE*, vol. 100, no. 10, pp. 2946–2970, 2012.

Silvana G. Dellepiane graduated in 1986 with honors. In 1990 she received the Ph.D. degree in electronic engineering and computer science.

In 1992, she became a Researcher (Assistant Professor) at Università degli Studidi Genova, where she is an Associate Professor in the ING_INF03 area, in the Department of Electrical, Electronic, Telecommunications Engineering and Naval Architecture (DITEN). She has taught in signal theory and pattern recognition. At present she is a Professor of electrical communications, statistical methods and telecommunication measures, signal and image processing and recognition, in the courses of electronics and telecommunications engineering and bioengineering. She is responsible for the NUMIP research area of the Signal Processing and Telecommunications (SP&T) Laboratory at DITEN (formerDIBE). Prof. Dellepiane has gained wide scientific and technical experience in multi-dimensional data processing. Her main research interests include use of context and fuzzy systems for multi-dimensional data processing, segmentation, supervised methods for the processing of remote sensing SAR images, and non-linear adaptive processing of digital signals. Her application domains are, mainly, telemedicine and remote sensing.

Prof. Dellepiane is a reviewer for various journals, including the IEEE TRANSACTIONS ON IMAGE PROCESSING, the IEE *Proceedings–I, Communications, Speech and Vision*, the IEE *Proceedings on Vision, Image and Signal Processing*, the *International Journal of Remote Sensing*, *Pattern Recognition*, and *Pattern Recognition Letters*. She was invited at some international conferences and schools for tutorial and lessons. She has participated, at organizational and scientific level, in research activities concerning various CNR, ASI, MIUR and UE projects. She is a member of the IEEE Technical Committee "Bio Imaging and Signal Processing" of the Signal Processing Society.

Elena Angiati was born in Novi Ligure, Italy, in 1981. She received the Laurea degree (B.Sc.) in February 2004 and the Laurea Magistrale degree (M.Sc.) in December 2006, both in telecommunications engineering, from University of Genoa, Italy. She developed her Master thesis on unsupervised change detection in remote sensing images by multiscale Markov random fields. Since January 2007, she has cooperated with NUMIP (NUmerical-IMage Processing) group at DIBE (Department of Biophysical and Electronic Engineering) in research activities concerning image processing and pattern recognition algorithms. In April 2011, she received the Ph.D. degree in space science and engineering; her research topics dealt with pattern recognition in remote sensing image processing for monitoring and security. Her research works are related with damage assessment for applications such as change detection by radar and optical data, coastline detection and flood monitoring. SAR and SAR interferometry data are used for data processing. She is co-author of some papers presented at international conferences.

Since October 2011, she works as Flight Control System Engineer for avionic and aeronautic multinational corporations.